Phosphoprotein and Phosphopeptide Interactions with the FHA Domain from Arabidopsis Kinase–Associated Protein Phosphatase †

9 AUTHORS, INCLUDING:

Fabio Gallazzi
University of Missouri
51 PUBLICATIONS **1,825** CITATIONS

Shashi Bhushan Pandit
Indian Institute of Science Education & Rese…
23 PUBLICATIONS **468** CITATIONS

Jeffrey Skolnick
Georgia Institute of Technology
391 PUBLICATIONS **17,207** CITATIONS

Steven R Van Doren
University of Missouri
60 PUBLICATIONS **1,390** CITATIONS

Phosphoprotein and Phosphopeptide Interactions with the FHA Domain from Arabidopsis Kinase-Associated Protein Phosphatase[†]

Zhaofeng Ding,[‡] Huachun Wang,[‡,§] Xiangyang Liang, Erin R. Morris,[§] Fabio Gallazzi,[‖] Shashi Pandit,[⊥]
Jeffrey Skolnick,[⊥] John C. Walker,*,[§] and Steven R. Van Doren*

*Department of Biochemistry, Division of Biological Sciences and Bond Life Sciences Center, University of Missouri,
Columbia, Missouri 65211*

Received August 25, 2006; Revised Manuscript Received November 14, 2006

ABSTRACT: FHA domains are phosphoThr recognition modules found in diverse signaling proteins, including kinase-associated protein phosphatase (KAPP) from *Arabidopsis thaliana*. The kinase-interacting FHA domain (KI-FHA) of KAPP targets it to function as a negative regulator of some receptor-like kinase (RLK) signaling pathways important in plant development and environmental responses. To aid in the identification of potential binding sites for the KI-FHA domain, we predicted (i) the structure of a representative KAPP-binding RLK, CLAVATA1, and (ii) the functional surfaces of RLK kinase domains using evolutionary trace analysis. We selected phosphopeptides from KAPP-binding Arabidopsis RLKs for in vitro studies of association with KI-FHA from KAPP. Three phosphoThr peptide fragments from the kinase domain of CLV1 or BAK1 were found to bind KI-FHA with K_D values of 8–20 μM, by NMR or titration calorimetry. Their affinity is driven by favorable enthalpy and solvation entropy gain. Mutagenesis of these three threonine sites suggests Thr546 in the C-lobe of the BAK1 kinase domain to be a principal but not sole site of KI-FHA binding in vitro. The brassinosteroid receptor BRI1 and KAPP are shown to associate in vivo and in vitro. Further genetic studies indicate that KAPP may be a negative regulator of the BRI1 signaling transduction pathway. ^{15}N-Labeled KI-FHA was titrated with the GST-BRI1 kinase domain and monitored by NMR. BRI1 interacts with the same 3/4, 4/5, 6/7, 8/9, and 10/11 recognition loops of KI-FHA, with similar affinity as the phosphoThr peptides.

Plants use receptor-like protein kinases (RLK)[1] to sense developmental signals and changing environmental conditions and to trigger signaling cascades to bring about developmental and adaptive responses (*1*). Genome research suggests 417 RLKs in Arabidopsis, most of which lack a demonstrated receptor function (*2*). However, where functions are known, RLKs play important roles in a wide variety of signaling contexts in plants such as self-incompatibility, hormonal signaling, nodulation, abscission, wound responses,

and disease resistance (*2*). RLKs such as CLAVATA1 (CLV1), brassinosteroid-insensitive kinase 1 (BRI1), and BRI1-associated kinase 1 (BAK1) are critical to plant growth and development (*3*–*7*). BRI1 and BAK1 are essential components of the brassinosteroid receptor (BR) in brassinosteroid-dependent signal transduction in Arabidopsis (*4*–*7*). CLV1, BRI1, and BAK1 are membrane-localized and belong to the leucine-rich repeat (LRR) family of RLKs of Arabidopsis. Each of these RLKs contains a receptor domain, a single transmembrane helix, and an intracellular serine/threonine protein kinase domain (*8, 9*).

Kinase-associated protein phosphatase (KAPP) is a downstream regulator of RLKs in Arabidopsis (*10*). No homologues of KAPP have been identified in the Arabidopsis genome (*11*). KAPP has a wide expression pattern and serves as a negative regulator of multiple RLK signal transduction pathways (*12, 13*). KAPP was found to interact with several Arabidopsis RLKs, including RLK5 or HAESA (*10*), RLK4 (*14*), CLV1 (*13*), FLS2 (*15*), and SERK1 (*16*). KAPP orthologues in maize and rice also bind several RLKs (*14*). KAPP interacts with RLKs autophosphorylated on serine and/or threonine residues (*12, 16*–*18*). KAPP contains the following domains: an N-terminal type I membrane anchor, a kinase-interacting FHA domain (KI-FHA), and a type 2C protein phosphatase (PP2C) domain (*10*). The minimal kinase-interacting FHA domain contains the 119 residues from 180 through 298 in KAPP numbering (*19*). The KI-FHA domain was shown to bind phosphorylated RLKs in

vitro and fails to bind dephosphorylated RLKs (*10*, *13*, *14*, *19*). It has been hypothesized that KAPP utilizes its KI-FHA domain to bind the phosphorylated RLK kinase domain to position the PP2C domain to dephosphorylate phosphoSer/Thr residues of RLK kinase domains on the intracellular face of the plasma membrane. This results in decreased RLK kinase activity and attenuated RLK signaling (*20*). Much of how KAPP binds some RLKs and how KAPP-RLK signaling complexes assemble remains unknown.

The FHA (forkhead-associated) domain is a class of phosphorylation-dependent protein−protein interaction domains with specificity for phosphoThr and conceivably phosphoSer. FHA domains have been found in more than 800 different proteins (http://smart.embl-heidelberg.de/) from both eukaryotes and some prokaryotes. Those proteins include DNA repair and checkpoint proteins, protein kinases, protein phosphatases, kinesins, and transcription factors. The regions of homology among FHA domains comprise 55−75 amino acids that are essential but not sufficient to form a functional phospholigand binding unit. Functional FHA domain modules usually contain 120−140 residues (*20*). The structures of several FHA domains have been solved (*21*−*25*). FHA domains have been shown to bind pThr peptides with strong and differing preferences for the residue in the pT +3 position of the peptides (*26*). For example, the FHA1 domain of yeast Rad53 selects a pTXXD peptide motif (*27*), and that of human Chk2 binds a pTXX(I/L) motif (*28*). Even with peptide library screening data available for the FHA domain of KAPP, it remains unclear what site(s) in an RLK are recognized by the KI-FHA of KAPP.

We searched for potential KI-FHA binding sites on KAPP-binding RLKs by screening peptide fragments of the kinase domains containing phosphoThr/Ser. We describe the association of three pThr peptides with KI-FHA, their location in the predicted structure of the kinase domain of an important RLK, and confirmation by mutagenesis that one of the three sites is a principal site of binding by KI-FHA in vitro. We also demonstrate that KAPP interacts with BRI1 in vivo and acts as a negative regulator in *A. thaliana*. In vitro, the FHA domain of KAPP interacts with the kinase domain of either BRI1 or BAK1. NMR-detected titrations indicate that the BRI1 kinase domain and phosphoThr peptides bind the same surface of KI-FHA with qualitatively similar affinity.

MATERIALS AND METHODS

Prediction of the Structure of the CLV1 Kinase Domain. Tertiary structure prediction of the CLV1 kinase domain was undertaken using the TASSER algorithm (*29*, *30*). The sequence of the CLV1 kinase domain was threaded against the template library using PROSPECTOR_3 (*31*). This provided the set of putative templates compatible with the sequence. TASSER extracted consensus-predicted side chain contacts from the threading templates as well as continuous fragments of structure provided by the threading alignments. A full-length model based on each template was constructed, and conformational space was searched using a variant of replica exchange Monte Carlo called parallel hyperbolic sampling (*32*). The 14 lowest temperature replicas were clustered using SPICKER (*33*), and the structure associated with the most populated cluster constituted the prediction.

TASSER was able to improve significantly the quality of the model relative to the starting target-template alignment (*29*). The side chain rebuilding program PULCHRA (manuscript in preparation) was used to generate a detailed atomic model subsequent to the prediction of the tertiary structure of the backbone.

Preparation of KI-FHA and GST Fusion with the BRI1 Kinase Domain. GST-tagged KI-FHA, containing residues 180−313 of Arabidopsis KAPP, was expressed in *Escherichia coli* and purified as described (*34*). The N-terminal GST tag was removed with 3C protease (PreScission; GE Healthcare).

The sequence encoding the kinase domain from residue 816 to residue 1196 of Arabidopsis BRI1 (GI: 2392895) was amplified by PCR and subcloned into the vector pET42a as described (*35*). The fusion protein was expressed in *E. coli* BL21 in LB medium for 3 h at 28 °C after induction with 250 μM IPTG. The following protease inhibitors were added to the cell lysate: 1 μM pepstatin A, 10 μM leupeptin, 0.1 mM TPCK, 0.5 mM AEBSF, and 5 μM E-64 (Sigma). After disrupting the *E. coli* culture with a French press, the soluble supernatant was dialyzed against PBS buffer (pH 7.4) to eliminate endogenous glutathione. The fraction was incubated with glutathione agarose (Sigma) at 4 °C. BRI1 was eluted with 30 mM reduced glutathione (Sigma) in 50 mM Hepes (pH 7.4). The purified GST-BRI1 kinase domain was dialyzed and concentrated to 0.36 mM (24.6 mg/mL) in 20 mM sodium phosphate (pH 6.3) with 120 mM NaCl and 7% D$_2$O for NMR-detected titration.

Isothermal Titration Calorimetry of the KI-FHA Interaction with PhosphoThr/Ser Peptides. Forty-three phosphopeptides (Table S1 of Supporting Information), chosen on the basis of the criteria described in Results, were synthesized as peptides with phosphorylation of the central threonine or serine as described (*36*). A positive control for KI-FHA binding was also synthesized using the idealized sequence of AAYAYpTQASAAKKK. The 44 phosphoThr/Ser peptides (40−70% pure) were initially assayed for binding to KI-FHA by ELISA and subsequently by isothermal titration calorimetry (ITC) (Table S1). Phosphopeptides that interact with KI-FHA were purified to >85% by HPLC and used for further ITC with KI-FHA from KAPP.

The experimental design and data analysis of ITC have been described (*37*−*40*). We used a VP-ITC microcalorimeter from MicroCal, Inc. Both the KI-FHA samples and pThr peptides which bind were dialyzed into PBS buffer (pH 7.5) prior to ITC, using Float-A-Lyzer devices with 500 Da cutoff (Spectrum Laboratories), to ensure constant pH. Titrations were conducted at 25 °C. GST-KI-FHA or free KI-FHA samples, with concentrations ranging from 0.03 to 0.1 mM, were placed in the sample cell. The phosphopeptide solutions, with concentrations in 5−10 molar excess over [KI-FHA], were placed in the syringe and repeatedly injected at constant intervals. A control titration was performed by titrating the phosphopeptide into buffer only, in order to estimate heat of mixing. Baseline correction was done by subtracting the heat changes from the peptide-to-buffer control titration from the peptide-to-KI-FHA titration. After baseline correction, the sigmoidal curves were fit to an equation for an association with one-binding site using MicroCal Origin version 5.0. This revealed ΔH, ΔG, $T\Delta S$, and stoichiometry (N-value) for the association (Table 1).

Table 1: Thermodynamics of Phosphopeptide Associations with KI-FHA Monitored by ITC and NMR

	pThr peptide			
	RLADGT(p)LVAVK aa307−317	PEYAYT(p)LKVDEKS aa863−875	ALLAT(p)QSSPMER aa542−553	AAYAYT(p)QASAAKKK
name, RLK	pT312 BAK1	pT868 CLV1	pT546 BAK1	control
K_D, μM (NMR)[a]	8.0 ± 1.6	20.0 ± 2.6	40.0 ± 4.5	3.4 ± 2.0
ΔG, kcal/mol (NMR)[a]	−6.9 ± 0.6	−6.3 ± 0.3	−5.9 ± 0.2	−7.4 ± 2.8
ΔG, kcal/mol (ITC)[b]	−7.1 ± 0.4	−6.5 ± 0.3	−6.8 ± 0.4	−7.4 ± 0.7
ΔH, kcal/mol	−4.3 ± 0.1	−4.5 ± 0.3	−3.3 ± 0.1	−5.6 ± 0.2
$-T\Delta S$, kcal/mol	−2.8 ± 0.2	−2.0 ± 0.3	−3.5 ± 0.1	−1.8 ± 0.2
N-value (ITC)[b]	0.81 ± 0.02	1.0 ± 0.05	0.79 ± 0.02	0.83 ± 0.01
K_D, μM (ITC)[b]	9.2 ± 1.1	16.0 ± 2.0	9.9 ± 1.3	4.0 ± 0.6

[a] NMR titrations were done at pH 6.3. [b] ITC experiments were done at pH 7.5.

^{15}N KI-FHA NMR Titrations with Phosphopeptides. ^{15}N-Labeled KI-FHA was prepared with a concentration of 0.53−0.6 mM in 20 mM sodium phosphate buffer (pH 6.3) with 120 mM NaCl and 9% D_2O. Phosphopeptides were dissolved in the same buffer. The pH of each phosphopeptide stock solution was measured using a pH microelectrode and adjusted to 6.3. Undissolved materials were removed by centrifugation. The concentrations of the peptide stock solutions were determined to be 7−8 mM by quantitative amino acid analysis. The purified phosphoThr peptides were then titrated into ^{15}N-labeled KI-FHA at 22 °C. A Varian Inova 600 MHz spectrometer was used with a high-sensitivity 5 mm ^{1}H (*41*) cryogenic probe with an actively shielded Z-gradient coil. A series of 2D ^{15}N TROSY spectra were collected with molar ratios of ^{15}N KI-FHA to peptide of 1:0, 1:0.25, 1:0.5, 1:0.75, 1:1, 1:1.33, 1:1.67, 1:2, 1:2.5, 1:3, and 1:4. NMR spectra were processed using NMRPipe 2.3 (*42*). The titration curves were analyzed using nonlinear regression analysis (*43*, *44*). Chemical shift changes of a KI-FHA residue were plotted against total [peptide] for each titration. Binding affinity was determined by fits to the equation:

$$\delta_{obs} - \delta_P =$$
$$(\delta_{PL} - \delta_P)\frac{(K_D + L_t + P_t) - \sqrt{(K_D + L_t + P_t)^2 - 4P_tL_t}}{2P_t}$$

$$(1)$$

P_t and L_t are the total concentrations of the protein ^{15}N KI-FHA and peptide ligand, respectively. δ_{obs} is the observed NMR peak position or chemical shift. δ_P and δ_{PL} are the chemical shifts of the free KI-FHA and the complex. K_D is the dissociation constant. Microcal Origin version 6.0 was used with its global fitting option to fit the binding isotherms of all affected residues' ^{1}H peak positions simultaneously.

Mapping Phosphopeptide and GST-BRI1 Binding Sites on KI-FHA by NMR. For mapping the sites on KI-FHA where the phosphopartners bind, the ^{15}N TROSY spectra in the absence and in 4-fold excess were compared. The chemical shift changes of the amide peaks were calculated as the radius:

$$\Delta w_{NH} = (\Delta w_H{}^2 + (\Delta w_N/6)^2)^{1/2} \qquad (2)$$

where Δw_H and Δw_N are the changes (in parts per million) in the ^{1}H and ^{15}N dimensions. The factor of 6 normalizes the shifts in the ^{15}N dimension down to the scale of the changes in the ^{1}H dimension. For mapping the site of binding of the RLK BRI1, ^{15}N TROSY spectra were collected at 22

°C and 600 MHz ^{15}N KI-FHA, free and in the presence of additions of the GST-BRI1 kinase domain. The conditions used in order of nominal KI-FHA to BRI1 ratio, [KI-FHA], and NMR signal averaging time were as follows: 1:0, 0.4 mM, 0.5 h; 1:0.25, 0.31 mM, 1 h; 1:0.5, 0.26 mM, 8 h; and 1:0.75, 0.22 mM, 32 h. With the greater additions of the GST-BRI1 kinase domain to KI-FHA, the GST-BRI1 kinase domain precipitated heavily.

Conformational Entropy Change upon Binding: Crude Estimates from NMR Order Parameters. NMR order parameters, S_{LZ}, are available for KI-FHA, free and bound to pT868 CLV1 (*36*). Changes of configurational entropy ΔS_{conf} between bound (B) and free (F) states were proposed to relate to the Lipari−Szabo order parameter S_{LZ} describing picosecond to nanosecond bond reorientations (*45*):

$$\Delta S_{conf} = S_{conf,B} - S_{conf,F} =$$
$$Nk \ln((3 - (1 + 8S_{LZ,B})^{1/2})/(3 - (1 + 8S_{LZ,F})^{1/2})) \quad (3)$$

where k is the Boltzmann constant and N is Avogadro's number. However, such estimates can only be considered qualitative due to many limitations listed by Arumugam et al. (*46*).

Far-Western and Co-immunoprecipitation Analysis. Site-directed mutations were introduced to the kinase domains of CLV1 and BAK1 using the QuikChange mutagenesis kit (Stratagene, catalog no. 200518) as described by the manufacturer. Sequencing confirmed the mutations. MBP-CLV1, MBP-mCLV1 (K720E), MBP-CLV1 (T868A), MBP-mBAK1 (K317E), GST-BAK1, GST-BAK1 (T312A), GST-BAK1 (T546A), MBP-BRI1, and MBP-mBRI1 (K911E) were expressed and purified as described (*47*). mCLV1 (K720E), mBAK1 (K317E), and mBRI1 (K911E) each harbor an inactivating mutation of a conserved lysine that renders the protein kinase unable to autophosphorylate. Purified MBP-BRI1 and MBP-mBRI1 (K911E) were autophosphorylated in vitro with nonradioactive ATP (*6*) and loaded onto identical SDS−PAGE gels. One gel was stained. The bands of the other gel were transferred onto nitrocellulose (NC) membrane. The NC membrane was then blocked with 5% nonfat milk (w/v) and rinsed with PBS-T buffer. GST-KI-FHA (1 μg) was added and incubated with the NC membrane overnight in 4 °C. Anti-glutathione S-transferase (Sigma) and anti-rabbit (Amersham) antibodies were used. Far-Western assays were also performed on the purified MBP-CLV1, MBP-mCLV1 (K720E), MBP-CLV1 (T868A), MBP-mBAK1 (K317E), GST-BAK1, GST-BAK1 (T312A), and GST-BAK1 (T546A) as described above, except that a polyclonal antibody directed against KAPP (*48*) was used.
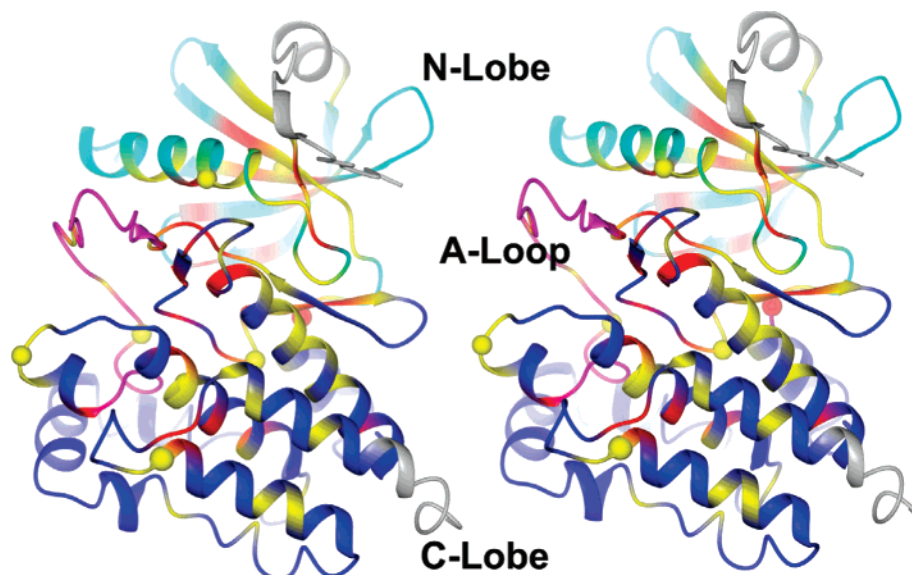
FIGURE 1: A stereoview of the predicted structure of the kinase domain of CLV1, representing LRR RLKs, is colored to mark regions predicted to be important for function. The backbone coordinates of this threaded structural model in PDB format can be downloaded from the Supporting Information. From the evolutionary trace analysis of LRR RLK kinase domains, the class-specific or subfamily-characteristic residues are colored yellow and the conserved residues red. Class-specific Thr/Ser residues are represented with yellow spheres and conserved ones with red spheres. The activation loop is in magenta. The N-lobe and C-lobe are colored cyan and blue, respectively. The N-terminal juxtamembrane region and C-terminal tail, defined previously (*17*, *60*), are in gray.

Co-immunoprecipitation experiments were performed with transgenic plants harboring 35S::BRI1-FLAG as described (*6*). Immunoprecipitated BRI1-FLAG was loaded onto identical SDS−PAGE gels and tested by Western blotting with anti-FLAG or anti-KAPP antibodies.

Root Growth Inhibition Assay with Brassinolide Treatment. The *kapp-3* T-DNA insertion allele, Garlic_125_D05, was generated by Syngenta. Primer sequences for genotyping of T-DNA insertion mutants are as follows: *kapp-3* 5′ primer, ATGTACTCTTAGAGTCTATCGACCAGT; *kapp-3* 3′ primer, AGACTAGATGGATGAGCTGTATCCTAT. The T-DNA insertion in *kapp-3* was followed by BASTA resistance and confirmed by PCR of genomic DNA. To genotype *bri1-5*, BRI1 was amplified by PCR with two primers: *bri1-5* 5′ primer, TCTGGTACCATGAAGAC-TTTTTCAAGCTTC; *bri1-5* 3′ primer, TCTGGTACCT-CATAATTTTCCTTCAGGAACTTC. The PCR product was for sequenced using the *bri1-5* 5′ primer.

Seeds freshly harvested from plants grown under 16 h light/8 h dark growth conditions were used for root growth inhibition analysis. The seeds were surface sterilized and planted on MS plates (0.7% agar, pH 5.7) containing different concentrations of epibrassinolide (eBR; Sigma), an active synthetic analogue of natural brassinolide. The plates were kept at 4 °C for 3 days and then treated with red light for 1 h to enhance uniform germination. The plates were kept in the dark for another 23 h. The plates were then placed vertically with yellow light illumination at 23 °C. Germination is generally considered to occur 23 h after red light treatment. The roots were photographed and measured 7 days after germination (*6*).

RESULTS

Structure and Functional Surfaces Predicted for the LRR RLK Protein Kinase Domain. No experimental structure of an RLK protein kinase domain has been reported. Such a

structural model would aid exploration of potential surfaces that KAPP might recognize. We elected to predict the tertiary structure of the kinase domain of CLV1 that has been well characterized in development, biochemistry, and recognition of KAPP (*48−54*). A threading template assembly/refinement approach known as TASSER was used. PROSPEC-TOR_3 identified a set of 20 relatively high-scoring, kinase-fold-related templates for the CLV1 kinase domain, whose consistency and Z-score suggested a quite reliable prediction. The highest scoring template has the Protein Data Bank identifier 1b6c (*55*), the serine/threonine protein kinase domain from type I TGFβ receptor. This template has 24% sequence identity with the CLV1 sequence. We note that functional inference should not be made on the basis of structural similarity alone. The resulting templates were passed to TASSER, and the most populated cluster consti-tutes the prediction. The quality of the best predicted model generated by TASSER is given by a confidence score or *C*-score (*30*). The *C*-score for the model generated for CLAVATA is 1.48. Based on the PDB benchmark (*30*), this *C*-score implies that the model has a greater than 98% probability to have backbone RMSD < 6.5 Å from the native structure. The model has about 85% of its residues in the most favored and allowed regions of the Ramachandran map. The ∼15% of residues with poor backbone geometry are restricted to loops and turns of the model, where prediction is known to be less reliable (*30*, *56*). According to the predicted structural model (Figure 1), the CLV1 kinase domain has two subdomains, the N-lobe and the C-lobe. The N-lobe contains a five-stranded β-sheet and two α-helices. The C-lobe begins with two helices followed by two central β-hairpins. Following the second β-hairpin in the C-lobe is the activation loop that precedes seven more α-helices.

For a set of 61 Arabidopsis RLKs, comprising the LRR II and LRR X−XIII families (*57*), we conducted evolutionary trace analysis to forecast regions of their kinase domains

important to function. This set includes these RLKs that interact with KAPP: CLV1, HAESA, SERK1, BAK1, and BRI1. The ET approach identifies "class-specific" sites that differ among subfamilies at functionally important sites (*58*), in this case among LRR RLKs. Such positions that systematically differ may tune the specificities that distinguish subfamilies (*58*, *59*). We reasoned that perhaps at least one of these loci might contribute to a KAPP binding site. At least ten class-specific segments are exposed on the surface of the structural model of the kinase domain of the representative family member CLV1 (Figure 1). The surface-exposed, class-specific sites are found in kinase subdomains I through V of the N-lobe, as well as subdomains VIa−IX and XI of the C-lobe (Figure S2 of Supporting Information). [The Roman numbering scheme for kinase subdomains has been described (*60*).]

Phosphopeptides from RLKs Screened for Interaction with the KI-FHA Domain of KAPP. We sought experimental evidence for sites on or near RLK kinase domains where the KI-FHA domain of KAPP might bind. Mapping using mutagenesis of RLK kinase domains from CLV1, HAESA, BAK1, or BRI1 expressed in *E. coli* was hampered by limited stability, solubility, level of expression, and sometimes by loss of protein kinase activity. We found that a phospho-peptide-directed approach made mapping more tractable. We screened candidate binding sites among KAPP-binding RLKs that include CLV1, BAK1, BRI1, FLS2, RLK4, and SERK1. As models of candidate binding sites for KI-FHA, we selected 43 threonine- or serine-containing peptides from their kinase domains (Table S1) and phosphorylated them during synthesis.

We selected a first set of threonine- or serine-containing sequences from BAK1 and CLV1 as candidates for phosphorylation and screening (Table S1 of Supporting Information). We considered four sequence criteria to suggest potential for KAPP binding. First, we favored sequences with residues in the pT −3 to pT +3 positions preferred by KAPP (*26*) (see legend of Table S1 of Supporting Information). Second, we favored threonines or serines found by evolutionary trace analysis to be class-specific, i.e., characteristic of RLK subfamilies (*58*) (Figure 1). Third, we only considered sequences where the threonine or serine is likely to be on the surface of the RLK and available to bind KAPP, judged by inspecting the structural model of CLV1 (Figure 1). Fourth, we preferred that a candidate's threonine or serine be conserved among most of the RLKs observed to bind KAPP, i.e., CLV1, HAESA, BAK1, BRI1, SERK1, WAK1, FLS2, and KIK1.

Reports of phosphorylation sites (*17*, *61*, *62*) suggested a second set of peptides for screening for affinity for KI-FHA. In vivo phosphorylation sites were identified in Arabidopsis membrane proteins that include ∼50 RLKs (*61*). Three-quarters of these phosphorylation sites in RLKs are in the juxtamembrane region (between the transmembrane helix and kinase domain) and at the C-terminus. In vitro and in vivo phosphoThr/Ser sites were identified in the recombinant BRI1 kinase domain (*17*, *62*). We considered threonine and serines of the C-terminal fragment of the FLS2 kinase domain reported to interact with KAPP (*15*) and reported to be phosphorylated in vivo (*61*).

None of the phosphopeptides selected from activation loops of RLKs interact with KI-FHA, i.e., pS848 CLV1, pT449 BAK1, pT450 BAK1, pT1039 BRI1, and pS1042 BRI1 (Table S1 of Supporting Information). This suggests that the activation loop may not be recognized by the KI-FHA domain portion of KAPP. Also, KI-FHA binds none of the peptides screened simply because they are known to be sites of phosphorylation (Table S1 of Supporting Information).

Location in RLKs of PhosphoThr Peptides That Bind KI-FHA. Three of the 43 peptides were found to have unambiguous affinity for KI-FHA (Table S1 of Supporting Information). These are phosphoThr peptides spanning residues 863−875 of CLV1 (named pT868 CLV1), residues 307−317 of BAK1 (named pT312 BAK1), and residues 542−553 of BAK1 (named pT546 BAK1) (Table 1). The locations of these three KI-FHA binding pThr peptides are marked on the CLV1 structural model (Figure 2a). pT312 BAK1 is located in the N-lobe at a loop and β-strand at the beginning of kinase subdomain II. The kinase subdomains are indicated on the alignment of RLKs in Figure S2 of Supporting Information. pT868 CLV1 lies in the C-lobe at the end of kinase subdomain VIII; this is in the first loop after the activation loop. Peptide pT546 BAK1 lies in kinase subdomain XI, closer to the C-terminus (Figure 2). All three of the peptides have residues (in pT −3 through pT +3 positions) observed to be preferred from a combinatorial library for binding KAPP (*26*). Notably, pT868 CLV1 and pT546 BAK1 coincide with sites suggested by evolutionary trace analysis to be important in function (Figures 1 and 2).

Energetics of Binding of Phosphopeptides to KI-FHA. The interactions of KI-FHA with the purified pThr peptides pT312 BAK1, pT546 BAK1, and pT868 CLV1 and a positive control pThr peptide were characterized by isothermal titration calorimetry (ITC). The positive control (Table 1) uses residues preferred in the pT −3 through pT +3 positions from the affinity assays of a combinatorial library (*26*); see Table S1 of Supporting Information. The titrations' raw binding isotherms and baseline-corrected, integrated points with best fits are displayed in Figure 3. The *N*-value of each of the titrations is near 1 (Table 1), suggesting 1:1 stoichiometry. At pH 7.5 and 25 °C, the dissociation constants between KI-FHA and the three phosphoThr peptides derived from RLKs range from 9 to 16 μM (Table 1). The K_D for KI-FHA and the control phosphoThr peptides with optimized sequence is 4 μM. The enthalpy change provides from about one-half to about three-quarters of the favorable free energy of association in each case (Table 1). The four pThr peptides bind KI-FHA with favorable entropic terms $-T\Delta S$ ranging from −1.8 to −3.5 kcal·mol^{-1} (Table 1).

The net entropy gain linked to binding is interesting considering the loss of entropy expected from the loss of freedom of diffusion on binding, loss of flexibility of the peptide once it binds, and the net increase of rigidity observed in the backbone of KI-FHA once pT868 CLV1 binds (*36*). We investigated whether release of ordered water might contribute to the entropy gain favoring the association. We performed calorimetric titrations of pT868 CLV1 with KI-FHA at 10, 14, 18, and 25 °C. ΔH_{obs} drops linearly with increasing temperature. ΔC_p from that slope is -230 ± 8 cal K^{-1} mol^{-1} (Figure S3 of Supporting Information). This ΔC_p can be used to estimate crudely the entropy of solvation from the expression $\Delta S_{solv} = \Delta C_p \ln(T/T_s^*)$, where T_s^* is
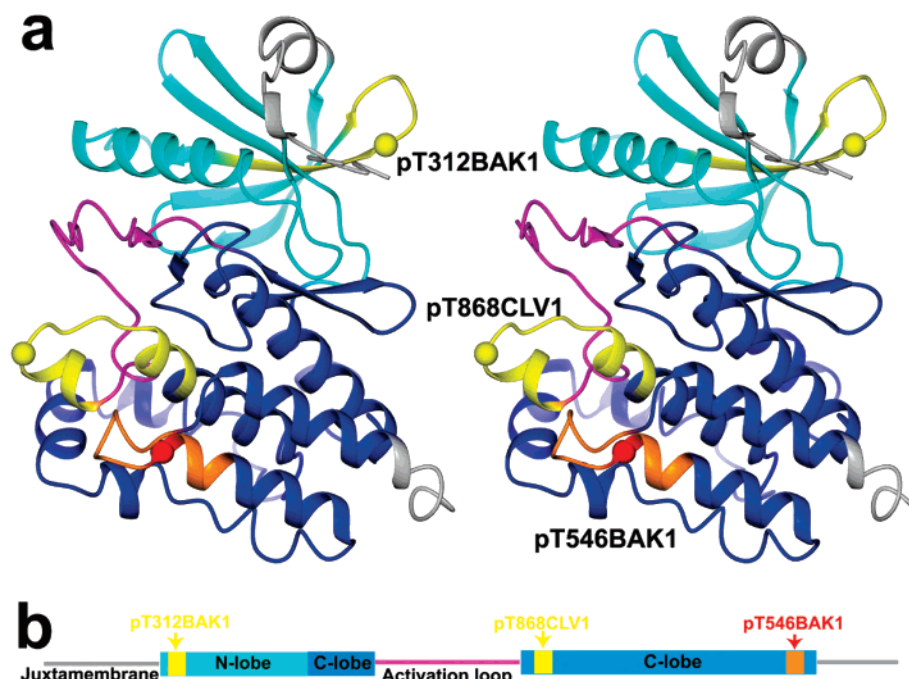
FIGURE 2: Locations within an RLK kinase domain of pThr peptides that bind KI-FHA are shown. Panel a shows the stereoview of the structure predicted for the representative CLV1 kinase domain. Panel b shows a cartoon of RLK kinase domains. Spheres correspond to threonines that were phosphorylated during peptide synthesis. The color code is the same as in Figure 1. Sites corresponding to BAK1 pT312 and CLV1 pT868 are in yellow. The T546 site of the intact BAK1 kinase domain suggested by mutagenesis to interact with KI-FHA in vitro is colored orange.
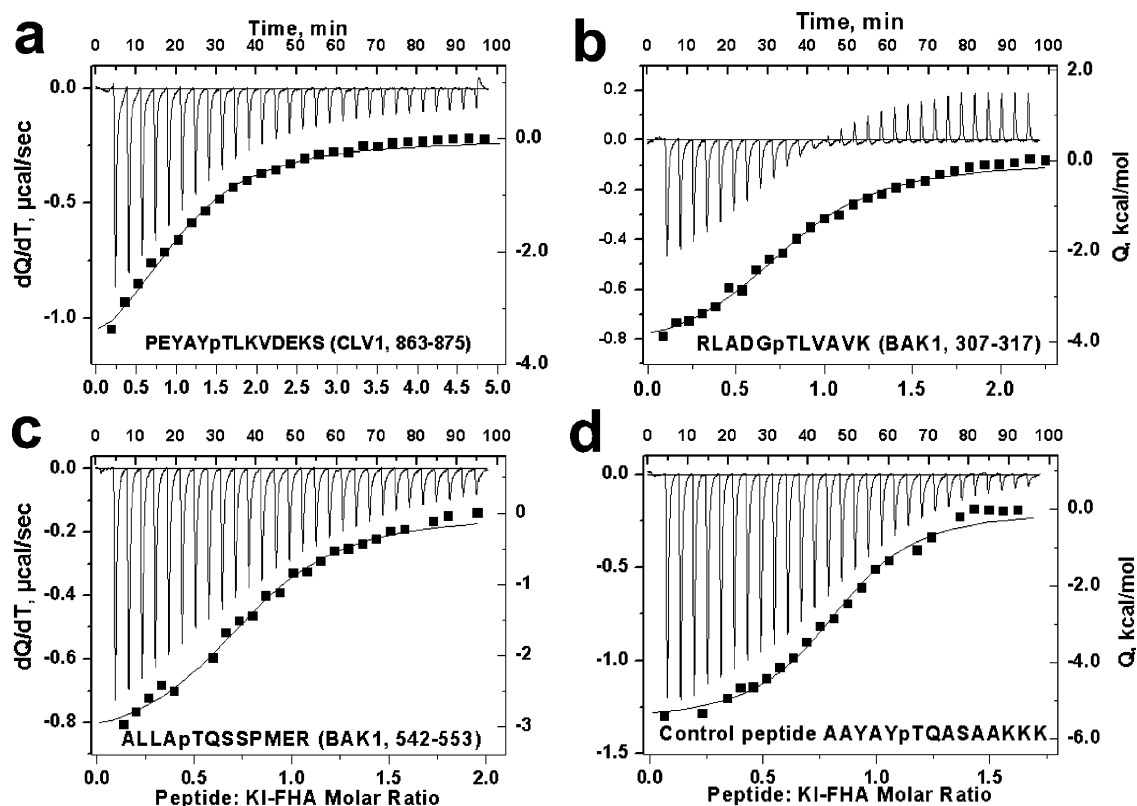

FIGURE 3: Calorimetric titrations with KI-FHA of the three phosphoThr peptides derived from RLKs. The upper trace and left axis of each panel describe the raw binding isotherms, while the lower squares and right axis describe the integrated heats. The pThr peptides include (a) pT868 CLV1, (b) pT312 BAK1, (c) pT546 BAK1, and (d) a positive control peptide with sequence of AAYAYpTQASAAKKK optimized from preferences reported from a library (26).

the reference of 385 K (63, 64). This suggests a rough estimate of the hydrophobic effect's contribution to the

entropy of binding at 25 °C of −18 kcal/mol. This is consistent with a large net release of ordered water molecules
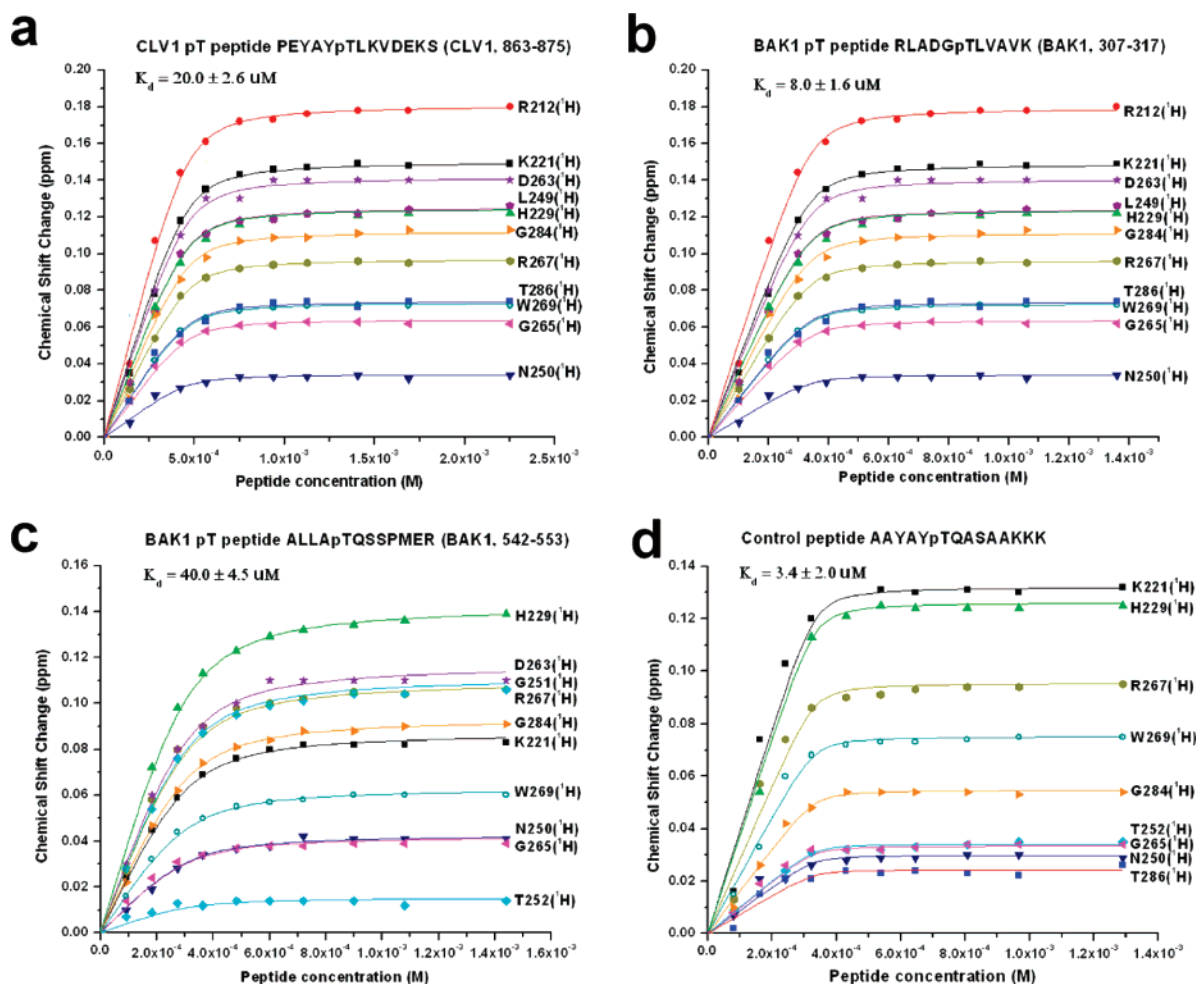
FIGURE 4: NMR-detected binding isotherms for the association of ^{15}N-labeled KI-FHA with (a) pT868 CLV1, (b) pT312 BAK1, (c) pT546 BAK1, and (d) the control peptide with sequence of AAYAYpTQASAAKKK. ^{1}H$_N$ chemical shift changes from ^{15}N TROSY spectra at pH 6.3 are plotted vs [peptide] for representative, affected residues. The fitted lines represent the global, simultaneous fit to the changes of all residues affected by that peptide. The color code for each residue is shared among the panels.

upon binding. This hydrophobic effect may be large enough to enhance affinity significantly, by offsetting the entropic costs from the increased structural rigidity in the complex.

Binding of Phosphopeptides to KI-FHA Characterized by NMR Titrations. We also monitored the affinity and binding sites of KI-FHA for the four phosphoThr peptides. A series of ^{15}N TROSY spectra were collected with ^{15}N KI-FHA-to-peptide molar ratios of 1:0, 1:0.25, 1:0.5, 1:0.75, 1:1, 1:1.33, 1:1.67, 1:2, 1:2.5, 1:3, and 1:4. In each NMR titration, the additions of the pThr peptides shifted progressively the amide peak positions of KI-FHA affected until ^{15}N KI-FHA was saturated (Figure 4). The binding isotherms were constructed by plotting ^{1}H chemical shift changes against total [peptide] (Figure 4); these two parameters are designated δ_{obs} and L_t, respectively, in eq 1. Each K_D was obtained by globally fitting each titration with eq 1. ^{15}N KI-FHA becomes saturated when each pThr peptide reaches about a 2-fold molar excess. The RLK-derived peptides bind ^{15}N KI-FHA with K_D values of 8−40 μM (Figure 4). The K_D with the control peptide is 3.4 μM. Despite the lower pH of 6.3, the NMR-derived Gibbs free energies of association agree within 0.2 kcal/mol with those from ITC, except for pT546 BAK1 (Table 1).

Recognition Loops of KI-FHA Perturbed by pThr Peptides. KI-FHA residues with large chemical shift changes cluster

at the apparent phosphopeptide binding site. The maximum amide peak shifts resulting from saturating additions of the pThr peptides were measured radially using eq 2. Binding of pT546 BAK1 peptide causes significant chemical shift changes at Gly211-Val213 of the 3/4 loop, Lys221-Asp222, Val225, and Gly227-His229 of the 4/5 loop, Met246 and Ser248-Thr252 of the 6/7 loop, Ser260, Asp263, Gly265, Arg267, and Trp269 of the 8/9 loop, and Gly284-Thr287 of the 10/11 loop (Figure 8a,d). Binding of the control pThr peptide causes peak shifts of similar size and location at Gly211-Val213 of the 3/4 loop, Lys221-Ser223, Val225, Gly227, and His229 of the 4/5 loop, Ser248-Gly251 of the 6/7 loop, Ser260, Asp263, Gly265, Arg267, and Trp269 of the 8/9 loop, and Gly284 and Thr286 of the 10/11 loop (Figure 8b,e). The pT312 BAK1 and pT868 CLV1 peptides cause similar effects on amide spectra of ^{15}N KI-FHA (*21, 36*). The 3/4, 4/5, 6/7, 8/9, and 10/11 loops are consistently implicated in the phosphopeptide recognition surface of KI-FHA, regardless of pThr peptide ligand.

Evaluation of the Three Prospective Binding Sites by Mutagenesis. We investigated whether any of the three pThr peptides identified correspond to a site that KI-FHA binds in an intact RLK protein kinase domain. We introduced single alanine substitutions for Thr868 of CLV1, Thr312 of BAK1, or Thr546 of BAK1. We screened a fusion protein

Table 2: Comparison of KI-FHA Binding by Threonine-Directed Mutations of the BAK1 Kinase Domain

	GST-BAK1	MBP-BAK1, inactivated by K317E[b]	GST-BAK1 T312A	GST-BAK1 T546A
relative capture of KI-FHA (%)[a]	100	6.5 ± 9	106 ± 57	38 ± 13

[a] $n = 3$. See Figure 5 for an example of one of the three replicates of far-Western assays quantified and averaged here. The density of the KI-FHA and antibody-probed RLK band was normalized by the density of the Coomassie-stained RLK band of an equally loaded companion gel. The normalized density is expressed as a percentage of the wild-type, positive control band. [b] Mutation of this conserved and essential lysine in protein kinases including RLKs abrogates activity (6). This lesion makes this construct a negative control, since autophosphorylation of the RLK's kinase domain is necessary for KI-FHA to bind.
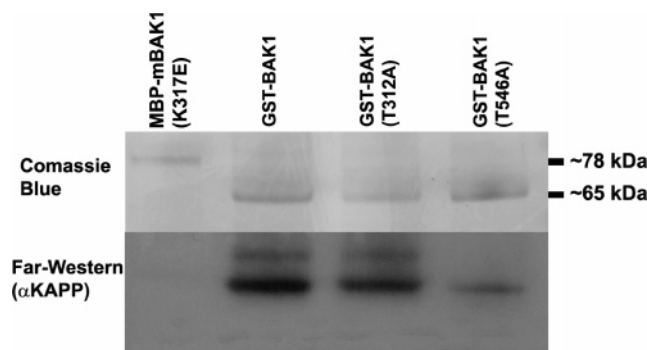

FIGURE 5: T546A substitution of BAK1 diminishes binding of KI-FHA. The affinity-purified fusion proteins of variants of the BAK1 kinase domain were run on duplicate SDS−PAGE gels (upper panel). The lower panel shows a far-Western blot in which one gel was electroblotted to the NC membrane, incubated with KI-FHA, and subsequently probed with antibody directed against KAPP.

with each mutation for interaction of the KAPP KI-FHA domain using far-Western detection with primary antibody against KAPP (48). The T868A mutant of MBP-CLV1 does not differ from wild-type MBP-CLV1 in capture of KI-FHA, within the sizable uncertainty resulting from low expression of soluble MBP-CLV1. Results are compared for fusion proteins of the BAK1 kinase domain with wild type, K317E-inactivated (negative control), T312A, and T546A variants (Table 2 and Figure 5). GST-BAK1 can clearly be seen to bind KI-FHA in vitro, but not the inactivated GST-BAK1 (K317) negative control. A more slowly migrating smear and band of GST-BAK1 recognized by KI-FHA suggests that autophosphorylation is present at more than two sites in the BAK1 kinase domain (Figure 5, lower panel). The T312A mutant is consistently equivalent to the wild-type BAK1 kinase domain in binding of KI-FHA, within the uncertainties. The T546A variant of BAK1, however, consistently retains only about 40% of the wild-type's extent of binding to KI-FHA. For *E. coli* expressed GST-BAK1 in vitro, the greatest share of KI-FHA from KAPP appears to bind at Thr546 in BAK1. Assuming that binding requires phosphorylation as reported (10), KI-FHA also appears to bind elsewhere in the recombinant BAK1 kinase domain.

KAPP binds to multiple RLKs in vitro (14). We were interested in examining KI-FHA's biochemical and genetic interactions with a related and important RLK that is known to interact with BAK1 in vivo.
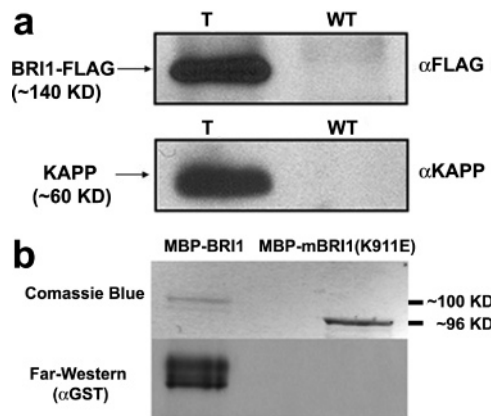

FIGURE 6: KAPP interacts with BRI1 in vivo and in vitro in a phosphorylation-dependent manner. (a) In vivo interaction. Total membrane proteins from transgenic Arabidopsis expressing BRI1-Flag (T) and nontransgenic Arabidopsis (WT) were immunoprecipitated (IP) with anti-FLAG M2 affinity gels. IP products, separated by gels and electroblotted to NC membranes identically, were detected with anti-Flag antibody (upper panel) or anti-KAPP antibody (lower panel). (b) In vitro interaction of the kinase domain of BRI1 with the KI-FHA domain from KAPP. Purified active MBP-BRI1 and inactive MBP-BRI1 (K911E) kinase domain fusions were loaded identically on SDS−PAGE gels. The upper panel shows Coomassie staining of one gel. The lower panel shows for the duplicate gel a far-Western blot of the NC membrane incubated with GST-KI-FHA and detected using an anti-GST antibody.

BRI1 Interacts with KAPP in Vivo and with KI-FHA in Vitro. Given the importance of BRI1 in plant development, we investigated whether KI-FHA from KAPP interacts with BRI1 in vivo. To test this, we performed co-immunoprecipitation experiments. The membrane fractions of transgenic Arabidopsis expressing BRI1-FLAG and wild-type (WT) Arabidopsis were incubated with anti-FLAG affinity gels. KAPP co-immunoprecipitated with BRI1-FLAG, suggesting that they interact in vivo (Figure 6a, lower panel). We examined whether the KI-FHA domain from KAPP interacts with the kinase domain of BRI1 in vitro, using far-Western detection. Maltose binding protein (MBP) fused with the kinase domain of either wild-type BRI1 (MBP-BRI1) or the K911E mutant of BRI1 (MBP-mBRI1) was prepared from *E. coli* and autophosphorylated in vitro. The K911E mutation abrogates kinase activity and autophosphorylation (62). When run on SDS−PAGE, autophosphorylated MBP-BRI1 migrates more slowly than unphosphorylated MBP-mBRI1 (K911E) (Figure 6b, upper panel). A duplicate gel was used for far-Western blotting, by incubating with GST-KI-FHA and subsequently with an antibody against GST. KI-FHA interacts with the active, phosphorylated MBP-BRI1 but not with inactivated MBP-mBRI1 (K911E) (Figure 6b, lower panel). This demonstrates that KI-FHA interacts with BRI1 in a phosphorylation-dependent manner. The smeared double-band in the far-Western blot of MBP-BRI1 suggests heterogeneity in phosphorylation (Figure 6b). The presumably heavier phosphorylation of the more slowly migrating band appears unnecessary for BRI1 to interact with KAPP.

KAPP Inhibits BRI1-Dependent Signaling. The functional significance of the interaction between KAPP and BRI1 was tested. A double mutant of *kapp-3/bri1-5* was generated. *kapp-3* is a T-DNA insertion line of Arabidopsis that harbors a T-DNA insertion in intron 1 of KAPP. *kapp-3* is both RNA-null and protein-null (Figure S1 of Supporting Information).
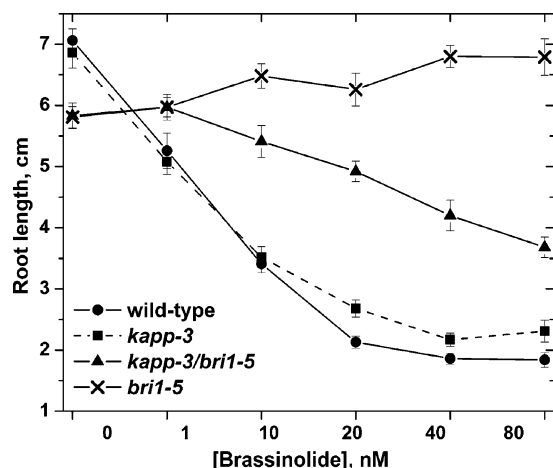
FIGURE 7: The effect of brassinolide on inhibition of root growth is quantified. Seedlings of wild-type, *kapp-3*, *bri1-5*, and *kapp-3/bri1-5* double mutants were germinated and grown on 1/2 Murashige and Skoog (MS) medium containing increasing concentrations of brassinolide. Root length was measured 7 days postgermination. Each data point represents the average root elongation of 40−50 seedlings. Error bars represent the standard error from the mean. The difference in inhibition of root elongation between *bri1-5* and the *bri1-5/kapp-3* double mutant is significant based on ANOVA. The same holds true for the wild type or *kapp-3* with the *bri1-5/kapp-3* double mutant. The difference in inhibition of root elongation between *kapp-3* and wild type is not significant.

bri1-5 is a weak *bri1* allele that retains partial function (*65*). No obvious growth and developmental phenotypes were observed in the *kapp-3/bri1-5* double mutants. To analyze the brassinolide sensitivity of the double mutant, we quantified root growth inhibition under brassinolide treatment. Brassinolide, like all other plant hormones, inhibits root growth at high concentrations. As shown in Figure 7, *bri1-5* is insensitive to brassinolide treatment up to 80 nM. The *kapp-3* null allele and wild type show no statistical difference in brassinolide sensitivity. Double mutant seedlings of *kapp-3/bri1-5* display sensitivity to brassinolide treatment that is intermediate between the insensitivity of *bri1-5* mutant seedlings and the sensitivity of wild-type or *kapp-3* seedlings. The root growth inhibition by brassinolide for the *kapp-3/bri1-5* and *bri1-5* mutant seedlings diverges between 1 and 80 nM brassinolide (Figure 7).

Surface of KI-FHA That Interacts with the Kinase Domain of BRI1. We used NMR to examine the interaction of an FHA domain with a large globular domain of a physiological phosphoprotein binding partner. For the globular partner, we selected the 43 kDa kinase domain of BRI1 shown in Figure 6 to interact with KAPP. We found BRI1 to be stable and soluble to 0.36 mM (25 mg/mL) when fused to GST. However, GST is well-known to dimerize, doubling the anticipated molecular mass of the GST-BRI1 construct to about 136 kDa. Association of such a large construct with ^{15}N-labeled KI-FHA of 15 kDa was expected to introduce considerable line broadening to amide spectra of KI-FHA. To compensate for such challenges, we exploited the ^{15}N line narrowing of ^{15}N TROSY detection, the high sensitivity of a cryogenic probe, and long signal averaging (see Materials and Methods for details). ^{15}N−^{1}H TROSY spectra of ^{15}N KI-FHA were collected without and with the addition of 0.25, 0.5 and 0.75 equiv of GST-BRI1. Since GST-BRI1 precipitated partially and increasingly with greater additions

to KI-FHA, the actual BRI1 to KI-FHA molar ratios were ≤0.25:1, <0.5:1, and <0.75:1. The size of the peak shifts in the KI-FHA spectrum increased with the additions of GST-BRI1, implying that the fast chemical exchange regime prevails. This suggests moderate affinity of GST-BRI1 for KI-FHA, similar to that observed in the pThr peptide titrations also in fast exchange. The radial chemical shift differences between ^{15}N TROSY spectra of free ^{15}N KI-FHA and KI-FHA in the presence of nominally 0.75 equiv of GST-BRI1 are plotted in Figure 8c. The smaller size of these chemical shift differences, compared to pThr peptide titrations, is consistent with the *inability* to saturate the KI-FHA with the GST-BRI1 at the high concentrations that exceeded 0.2 mM for KI-FHA. Significant chemical shift changes of KI-FHA residues occurred at Gly211-Arg212 of the 3/4 loop, Leu220-Asp222, Val225, and Lys228-His229 of the 4/5 loop, Asp245-Ser248 and Asn250 of the 6/7 loop, His261, Asp263-Gly265, and Arg267 of the 8/9 loop, and Leu283, Thr285-Thr286, and Lys288 of the 10/11 loop (Figure 8c,f). Thus, the surface of KI-FHA that binds the BRI1 kinase domain is composed of the same 3/4, 4/5, 6/7, 8/9, and 10/11 loops that bind the pThr peptides. In addition, the BRI1 construct introduces small chemical shift perturbations distant from this surface at the far ends of β-strands 3, 8, 9, and 11 and neighboring 7/8 and 9/10 loops. These peak shifts far from the main binding surface suggest either conformational adjustment at long range or perhaps some nonspecific interaction.

DISCUSSION

Significance of the BRI1 Interaction with KAPP and Its KI-FHA Domain. BRI1 possesses the most important brassinosteroid binding activity in Arabidopsis (*66*). Throughout a plant's lifetime, brassinosteroids regulate growth and differentiation. How BRI1 is deactivated is important in regulating extent and length of signaling triggered by brassinosteroid reception but is poorly understood (*66*). Importantly, BRI1 interacts with KAPP in vivo (Figure 6a). KAPP appears to limit the response of the weakly active *bri1-5* allele in brassinolide-sensitive root growth (Figure 7). The loss of KAPP activity in the *kapp-3/bri1-5* double mutants presumably allows the *bri1-5*-impaired activity of the BR receptor to remain unmodified by KAPP. The results suggest that KAPP may serve as a negative regulator of BRI-dependent signal transduction. KAPP's interaction with and negative regulation of other RLKs distinguishes it from BKI1 that was very recently reported to be a specific inhibitor of BRI1 (*67*).

The protein kinase domain of BRI1 and the KI-FHA domain are sufficient for the interaction in vitro (Figures 6b and 8c,f). KI-FHA's binding site and qualitative affinity for the BRI1 kinase domain are much like that for pThr peptides from homologous KAPP-interacting LRR RLKs (Figure 8). This suggests that pThr peptides are in some respects adequate as small-molecule mimics of RLK kinase binding to KI-FHA.

Prospective Binding Site for KI-FHA in the C-Lobe of BAK1. Mutagenesis of the Thr546 site of BAK1 appears to disrupt reproducibly more than half of KI-FHA binding to the BAK1 kinase domain expressed in *E. coli*. This binding occurs despite the *appearance* that Thr546 may be partly
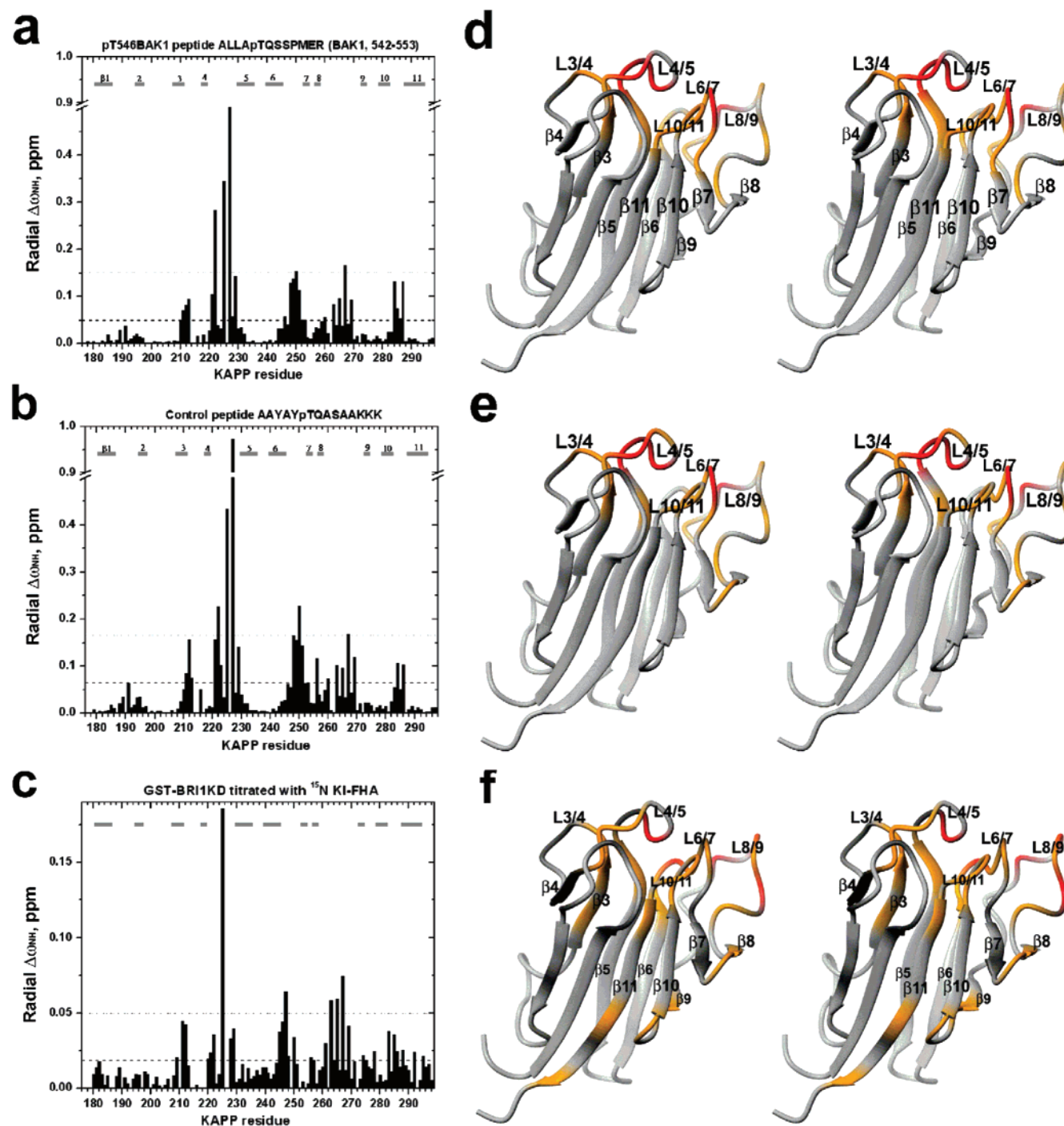
FIGURE 8: PhosphoThr peptides and the BRI1 kinase domain are recognized by the same surface of KI-FHA. Maximal binding-dependent changes observed in amide NMR peak shifts are plotted vs KAPP residue number for the pT546 BAK1 peptide at saturation (a), the control peptide at saturation (b), and 0.75 (nominal) equiv of GST-BRI1/equiv of KI-FHA (c). The binding-induced changes are plotted as radial shifts $\Delta\omega_{NH}$ according to eq 2. Sites of binding-induced peak shifts $\Delta\omega_{NH}$ are mapped onto the stereoview of the backbone ribbon of the free KI-FHA structure. KI-FHA residues are colored red where $\Delta\omega_{NH} > 0.15$ and yellow where $0.15 > \Delta\omega_{NH} > 0.05$ (d). Residues are colored red where $\Delta\omega_{NH} > 0.165$ and yellow where $0.165 > \Delta\omega_{NH} > 0.065$ (e). Residues are colored red where $\Delta\omega_{NH} > 0.05$ and yellow where $0.05 > \Delta\omega_{NH} > 0.0188$ (f). Unobserved residues are colored a darker shade of gray.

buried and only partly exposed on the surface of the predicted structural model in Figure 2. The phosphorylation of Thr546 is unlikely to allow this side chain to remain buried, due to its charge. Presumably phosphorylated Thr546 actually is on the surface, either due to its charge or due to uncertainty inherent to the predicted structural model. The Thr546 site in the C-lobe lies on the same side of the BAK1 kinase domain as the activation loop. This prospective binding site for the FHA domain would place its neighboring PP2C

domain from KAPP very well for dephosphorylating the activation loop of the kinase. Considering the length and potential flexibility of the linker joining the FHA and PP2C domains of KAPP (21), the in vitro binding site for KI-FHA seems neither too close nor too far from the activation loop of BAK1 for the PP2C domain to reach easily the activation loop. The Thr546 position is conserved with KAPP-binding RLKs HAESA, SERK1, WAK1, and FLS2, but not with BRI1 or CLV1 (Figure S2 of Supporting Information). The

prospective KAPP binding site in the C-lobe of one or more RLKs is consistent with the precedent of diverse protein kinases being inhibited by protein partners docked to their respective C-lobes (*68*).

Almost 40% of KI-FHA binding signal remaining using T546A-substituted BAK1 (Table 2) suggests that KI-FHA may bind to one or more other phosphorylated sites as well. The three phosphopeptide fragments of RLKs found to bind KI-FHA are consistent with its ability to bind some breadth of sequences. Isolated KI-FHA is monomeric (*36*). Yet it is possible that full-length KAPP might form a dimer with its dimeric RLK partner. If so, the FHA domain of a second chain of KAPP in a complex might be able to bind an additional and different region of an RLK.

Phosphopeptides That Fail To Bind KI-FHA May Narrow Down Alternatives for Binding Sites. About 75% of the sites of flagellin-elicited phosphorylation of RLKs in vivo were found in the juxtamembrane and C-terminal regions (*61*). Those observations, coupled with the importance of the phosphorylated juxtamembrane region of type I TGF beta receptor in a regulatory interaction with an FHA-like domain of SMAD2 (*69*), suggested the question: Might KI-FHA of KAPP interact analogously with phosphorylated juxtamembrane domains of RLK partners? PhosphoThr/Ser peptides from BRI1 corresponding to its sites of phosphorylation in the juxtamembrane region (*17*, *62*) show at best only very weak and ambiguous binding to KI-FHA (Table S1 of Supporting Information). This casts considerable doubt on the juxtamembrane region binding KAPP. C-Terminal phosphoSer peptides from FLS2 are similarly marginal in affinity for KI-FHA. The phosphorylated peptides from activation loop sequences we screened failed to bind KI-FHA as well; see S852, S857 of CLV1 and T449, T450, T455 of BAK1 in Table S1 of Supporting Information. A lack of involvement of the activation loop of an RLK in binding KI-FHA is further supported by alanine substitution of any threonine of BAK1's activation loop retaining full affinity for KI-FHA by far-Western blot (Table S2 of Supporting Information). To sum up, the known sites of RLK phosphorylation in juxtamembrane, activation loop, and C-terminal regions that we tested lack affinity for KI-FHA.

Energetics of pThr Peptide Binding to KI-FHA. The Gibbs free energy of pThr peptide affinity for KI-FHA, with K_D values of the order of 10 μM, comes at least half from favorable enthalpy of binding (Table 1). The favorable enthalpy can be attributed to optimal van der Waals close contacts, hydrogen bonding, and electrostatics at the interface. The KI-FHA residues (conserved or near the pT +3 site) that are most important for affinity for phosphopartners are remarkably rigid (*36*). Such rigidity was hypothesized to promote enthalpically favorable van der Waals contacts with the phosphopeptide (*36*, *70*, *71*).

It is noteworthy that the affinities of the pThr peptides for KI-FHA are also entropically favored. This comes despite the unfavorable entropic costs of flexible peptide becoming more rigid upon binding, the loss in diffusional degrees of freedom, and the net increase in rigidity of the backbone of KI-FHA (*36*). Just the entropic cost, ΔS_{conf}, of increased rigidity of KI-FHA upon binding is considerable. This entropic contribution $-T\Delta S_{conf}$ is estimated qualitatively to be 14 kcal/mol unfavorable, using eq 3 and the reported changes in rigidity of KI-FHA upon binding pT868 CLV1

(*46*). Even though such an estimate is very crude due to several limitations (*46*), it is sufficient to point out a significant energetic impediment to binding of the pThr peptide. How can this cost be paid such that the entropic term actually reverses and promotes binding? This cost would appear to be paid by a still larger favorable entropy gain, perhaps worth roughly -18 kcal/mol (see above), from ordered waters released upon binding. The large size of this solvation entropy and the heat capacity may raise a question as to whether water is released from sites in addition to the interface. It appears that the favorable hydrophobic effect may suffice to overcome the increased rigidity of KI-FHA to provide net entropy gain to promote binding.

Attributes Predictive of the KI-FHA Binding Site in an RLK. The success in finding a prospective KI-FHA binding site in an RLK kinase domain via three phosphopeptides found to bind KI-FHA provides a retrospective on the best sequence predictors. Sequence similarity to KAPP's residue preferences among a library of pThr peptides (*26*) (Table S1 of Supporting Information) clearly correlates with the phosphopeptides found to bind KI-FHA. Of the three best phosphopeptide ligands found for KI-FHA, the one that best matches the reported preferences in the pT +1 and pT +3 positions (*26*), i.e., T546 from BAK1, is the only site confirmed by mutagenesis to date to be a binding site in an intact RLK kinase domain in vitro. Evolutionary trace analysis also anticipated the functional importance of the binding site found at Thr546 of BAK1. ET also suggests functional importance of the Thr868 segment of CLV1 not confirmed by assay of the lone T868A point mutant. ET has been very successful in predicting functional sites (*59*, *72*) and can be applied more readily than screening of peptide libraries (*73*, *74*).

In summary, KAPP binds and negatively regulates BRI1 in vivo (Figures 6 and 7). The surface of KI-FHA from KAPP that recognizes BRI1's kinase domain coincides with the surface that recognizes phosphoThr peptides (Figure 8). The affinity of phosphoThr peptides is driven by the enthalpy of favorable contacts and probably also by the hydrophobic effect. KI-FHA failed to bind phosphopeptides tested from either the activation loop of three RLKs or the phosphorylated sites of the juxtamembrane region of BRI1 (Table S1 of Supporting Information). Instead, KI-FHA in vitro appears to bind Thr546 from BAK1, in the C-lobe on the same side of the kinase domain as the activation loop (Figures 2 and 5 and Table 2). This prospective binding site for the FHA domain of KAPP seems suited to support positioning of the PP2C domain of KAPP strategically for dephosphorylation of BAK1's activation loop.

SUPPORTING INFORMATION AVAILABLE

Three figures, three tables, and the set of predicted PDB coordinates for the backbone of the kinase domain of CLV1 are available. Figure S1 describes the *kapp-3* null allele.

Figure S2 shows the sequence alignment of KAPP-binding RLK kinase domains. Figure S3 shows the measurement of ΔC_p of the association of the CLV1 pT868 peptide with KI-FHA. Table S1 summarizes the characteristics of the pThr and pSer peptides screened for affinity for KI-FHA. Tables S2 and S3 compare KI-FHA interactions of BAK1 and CLV mutants that retain affinity for it. This material is available free of charge via the Internet at http://pubs.acs.org.

REFERENCES

1. Morris, E. R., and Walker, J. C. (2003) Receptor-like protein kinases: the keys to response, *Curr. Opin. Plant Biol. 6*, 339−342.

2. Becraft, P. W. (2002) Receptor kinase signaling in plant development, *Annu. Rev. Cell. Dev. Biol. 18*, 163−192.

3. Clark, S. E., Running, M. P., and Meyerowitz, E. M. (1993) CLAVATA1, a regulator of meristem and flower development in Arabidopsis, *Development 119*, 397−418.

4. Wang, Z. Y., Seto, H., Fujioka, S., Yoshida, S., and Chory, J. (2001) BRI1 is a critical component of a plasma-membrane receptor for plant steroids, *Nature 410*, 380−383.

5. Li, J. (2005) Brassinosteroid signaling: from receptor kinases to transcription factors, *Curr. Opin. Plant Biol. 8*, 526−531.

6. Li, J., Wen, J. Q., Lease, K. A., Doke, J. T., Tax, F. E., and Walker, J. C. (2002) BAK1, an Arabidopsis LRR receptor-like protein kinase, interacts with BRI1 and modulates brassinosteroid signaling, *Cell 110*, 213−222.

7. Nam, K. H., and Li, J. (2002) BRI1/BAK1, a receptor kinase pair mediating brassinosteroid signaling, *Cell 110*, 203−212.

8. Braun, D. M., and Walker, J. C. (1996) Plant transmembrane receptors: new pieces in the signaling puzzle, *Trends Biochem. Sci. 21*, 70−73.

9. Li, J., and Chory, J. (1997) A putative leucine-rich repeat receptor kinase involved in brassinosteroid signal transduction, *Cell 90*, 929−938.

10. Stone, J. M., Colinge, M. A., Smith, R. D., Horn, M. A., and Walker, J. C. (1994) Interaction of a protein phosphatase with an Arabidopsis serine-threonine receptor kinase, *Science 266*, 793−795.

11. Kerk, D., Bulgrien, J., Smith, D. W., Barsam, B., Veretnik, S., and Gribskov, M. (2002) The complement of protein phosphatase catalytic subunits encoded in the genome of Arabidopsis, *Plant Physiol. 129*, 908−925.

12. Stone, J. M., Trotochaud, A. E., Walker, J. C., and Clark, S. E. (1998) Control of meristem development by CLAVATA1 receptor kinase and kinase-associated protein phosphatase interaction, *Plant Physiol. 117*, 1217−1225.

13. Williams, R. W., Wilson, J. M., and Meyerowitz, E. M. (1997) A possible role for kinase-associated protein phosphatase in the Arabidopsis CLAVATA1 signaling pathway, *Proc. Natl. Acad. Sci. U.S.A. 94*, 10467−10472.

14. Braun, D. M., Stone, J. M., and Walker, J. C. (1997) Interaction of the maize and Arabidopsis kinase interaction doamins with a subset of receptor-like protein kinases: implication for transmembrane signaling in plants, *Plant J. 12*, 83−95.

15. Gómez-Gómez, L., Bauer, Z., and Boller, T. (2001) Both the extracellular leucine-rich repeat domain and the kinase activity of FLS2 are required for flagellin binding and signaling in Arabidopsis, *Plant Cell 13*, 1155−1163.

16. Shah, K., Russinova, E., Gadella, T. W., Jr., Willemse, J., and De Vries, S. C. (2002) The Arabidopsis kinase-associated protein phosphatase controls internalization of the somatic embryogenesis receptor kinase 1, *Genes Dev. 16*, 1707−1720.

17. Wang, X., Goshe, M. B., Soderblom, E. J., Phinney, B. S., Kuchar, J. A., Li, J., Asami, T., Yoshida, S., Huber, S. C., and Clouse, S. D. (2005) Identification and functional analysis of in vivo phosphorylation sites of the Arabidopsis brassinosteroid-insensitive1 receptor kinase, *Plant Cell 17*, 1685−1703.

18. Shah, K., Vervoort, J., and de Vries, S. C. (2001) Role of threonines in the *Arabidopsis thaliana* somatic embryogenesis receptor kinase 1 activation loop in phosphorylation, *J. Biol. Chem. 276*, 41263−41269.

19. Li, J., Smith, G. P., and Walker, J. C. (1999) Kinase interation domain of kinase-associated protein phosphatase, a phospho-ptotein-binding domain, *Proc. Natl. Acad. Sci. U.S.A. 96*, 7821−7826.

20. Li, J., Lee, G. I., Van Doren, S. R., and Walker, J. C. (2000) Commentary−The FHA domain mediates phosphoprotein interactions, *J. Cell Sci. 113*, 4143−4149.

21. Lee, G. I., Ding, Z., Walker, J. C., and Van Doren, S. R. (2003) NMR structure of the forkhead-associated domain from the Arabidopsis receptor kinase-associated protein phosphatase, *Proc. Natl. Acad. Sci. U.S.A. 100*, 11261−11266.

22. Liao, H., Byeon, I. J., and Tsai, M. D. (1999) Structure and function of a new phosphopeptide-binding domain containing the FHA2 of Rad53, *J. Mol. Biol. 294*, 1041−1049.

23. Liao, H., Yuan, C., Su, M. I., Yongkiettrakul, S., Qin, D., Li, H., Byeon, I. J., Pei, D., and Tsai, M. D. (2000) Structure of the FHA1 domain of yeast Rad53 and identification of binding sites for both FHA1 and its target protein Rad9, *J. Mol. Biol. 304*, 941−951.

24. Li, J., Williams, B. L., Haire, L. F., Goldberg, M., Wilker, E., Durocher, D., Yaffe, M. B., Jackson, S. P., and Smerdon, S. J. (2002) Structural and functional versatility of the FHA domain in DNA-damage signaling by the tumor suppressor kinase Chk2, *Mol. Cell 9*, 1045−1054.

25. Stavridi, E. S., Huyen, Y., Loreto, I. R., Scolnick, D. M., Halazonetis, T. D., Pavletich, N. P., and Jeffrey, P. D. (2002) Crystal structure of the FHA domain of the Chfr mitotic checkpoint protein and its complex with tungstate, *Structure 10*, 891−899.

26. Durocher, D., Taylor, I. A., Sarbassova, D., Haire, L. F., Westcott, S. L., Jackson, S. P., Smerdon, S. J., and Yaffe, M. B. (2000) The molecular basis of FHA domain:phosphopeptide binding specificity and implications for phospho-dependent signaling mechanisms, *Mol. Cell 6*, 1169−1182.

27. Yuan, C., Yongkiettrakul, S., Byeon, I, J, Zhou, S., and Tsai, M. D. (2001) Solution structures of two FHA1-phosphothreonine peptide complexes provide insight into the structural basis of the ligand specificity of FHA1 from yeast Rad53, *J. Mol. Biol. 314*, 563−575.

28. Qin, D., Lee, H., Yuan, C., Ju, Y., and Tsai, M. D. (2003) Identification of potential binding sites for the FHA domain of human Chk2 by in vitro binding studies, *Biochem. Biophys. Res. Commun. 311*, 803−808.

29. Zhang, Y., Arakaki, A. K., and Skolnick, J. (2005) TASSER: An automated method for the prediction of protein tertiary structures in CASP6, *Proteins*.

30. Zhang, Y., and Skolnick, J. (2004) Automated structure prediction of weakly homologous proteins on a genomic scale, *Proc. Natl. Acad. Sci. U.S.A. 101*, 7594−7599.

31. Skolnick, J., Kihara, D., and Zhang, Y. (2004) Development and large scale benchmark testing of the PROSPECTOR_3 threading algorithm, *Proteins 56*, 502−518.

32. Zhang, Y., Kihara, D., and Skolnick, J. (2002) Local energy landscape flattening: parallel hyperbolic Monte Carlo sampling of protein folding, *Proteins 48*, 192−201.

33. Zhang, Y., and Skolnick, J. (2004) SPICKER: a clustering approach to identify near-native protein folds, *J. Comput. Chem. 25*, 865−871.

34. Lee, G., Li, J., Walker, J. C., and Van Doren, S. R. (2003) ^{1}H, ^{13}C and ^{15}N resonance assignments of kinase-interacting FHA domain from Arabidopsis phosphatase KAPP, *J. Biomol. NMR 25*, 253−254.

35. Wang, X. L. X., Meisenhelder, J., Hunter, T., Yoshida, S., Asami, T., and Chory, J. (2005) Autoregulation and homodimerization are involved in the activation of the plant steroid receptor BRI1, *Dev. Cell 8*, 855−865.

36. Ding, Z., Lee, G.-I., Liang, X., Gallazzi, F., Arunima, A., and Van Doren, S. R. (2005) PhosphoThr peptide binding globally rigidifies much of the FHA domain from Arabidopsis receptor kinase-associated protein phosphatase, *Biochemistry 44*, 10119−10134.

37. Wiseman, T., Williston, S., Brandts, J. F., and Lin, L. N. (1989) Rapid measurement of binding constants and heats of binding using a new titration calorimeter, *Anal. Biochem. 179*, 131−137.

38. Pierce, M. M., Raman, C. S., and Nall, B. T. (1999) Isothermal titration calorimetry of protein-protein interactions, *Methods 19*, 213−221.

39. Doyle, M. L. (1997) Characterization of binding interactions by isothermal titration calorimetry, *Curr. Opin. Biotechnol. 8*, 31−35.

40. Fisher, H. F., and Singh, N. (1995) Calorimetric methods for interpreting protein-ligand interactions, *Methods Enzymol. 259*, 194−221.

41. Boelens, R., Burgering, M., Fogh, R. H., and Kaptein, R. (1994) Time-saving methods for heteronuclear multidimensional NMR of (^{13}C/^{15}N) doubly labeled proteins, *J. Biomol. NMR 4*, 201−213.

42. Delaglio, F., Grzesiek, S., Vuister, G. W., Zhu, G., Pfeifer, J., and Bax, A. (1995) NMRPipe: a multidimensional spectral processing system based on UNIX pipes, *J. Biomol. NMR 6*, 277−293.

43. Ferreon, J. C., and Hilser, V. J. (2003) Ligand-induced changes in dynamics in the RT loop of the C-terminal SH3 domain of Sem-5 indicate cooperative conformational coupling, *Protein Sci. 12*, 982−996.

44. Lian, L., and Roberts, G. C. K. (1993) in *NMR of Macromolecules. A practical approach* (Roberts, G. C. K., Ed.) pp 153−182, Oxford University Press, Oxford, U.K.

45. Yang, D., and Kay, L. E. (1996) Contributions to conformational entropy arising from bond vector fluctuations measured from NMR-derived order parameters: application to protein folding, *J. Mol. Biol. 263*, 369−382.

46. Arumugam, S., Gao, G., Patton, B. L., Semenchenko, V., Brew, K., and Van Doren, S. R. (2003) Increased backbone mobility in β-barrel enhances entropy gain driving binding of N-TIMP-1 to MMP-3, *J. Mol. Biol. 327*, 719−734.

47. Horn, M. A., and Walker, J. C. (1994) Biochemical properties of the autophosphorylation of RLK5, a receptor-like protein kinase from *Arabidopsis thaliana*, *Biochim. Biophys. Acta 1208*, 65−74.

48. Stone, J. M., Trotochaud, A. E., Walker, J. C., and Clark, S. E. (1998) Control of meristem development by CLAVATA1 receptor kinase and kinase-associated protein phosphatase interactions, *Plant Physiol. 117*, 1217−1225.

49. Dievart, A., Dalal, M., Tax, F. E., Lacey, A. D., Huttly, A., Li, J., and Clark, S. E. (2003) CLAVATA1 dominant-negative alleles reveal functional overlap between multiple receptor kinases that regulate meristem and organ development, *Plant Cell 15*, 1198−1211.

50. DeYoung, B. J., and Clark, S. E. (2001) Signaling through the CLAVATA1 receptor complex, *Plant Mol. Biol. 46*, 505−513.

51. Trotochaud, A. E., Jeong, S., and Clark, S. E. (2000) CLAVATA3, a multimeric ligand for the CLAVATA1 receptor-kinase, *Science 289*, 613−617.

52. Jeong, S., Trotochaud, A. E., and Clark, S. E. (1999) The Arabidopsis CLAVATA2 gene encodes a receptor-like protein required for the stability of the CLAVATA1 receptor-like kinase, *Plant Cell 11*, 1925−1934.

53. Clark, S. E., Williams, R. W., and Meyerowitz, E. M. (1997) The CLAVATA1 gene encodes a putative receptor kinase that controls shoot and floral meristem size in Arabidopsis, *Cell 89*, 575−585.

54. Williams, R. W., Wilson, J. M., and Meyerowitz, E. M. (1997) A possible role for kinase-associated protein phosphatase in the Arabidopsis CLAVATA1 signaling pathway, *Proc. Natl. Acad. Sci. U.S.A. 94*, 10467−10472.

55. Berman, H. M., Battistuz, T., Bhat, T. N., Bluhm, W. F., Bourne, P. E., Burkhardt, K., Feng, Z., Gilliland, G. L., Iype, L., Jain, S., Fagan, P., Marvin, J., Padilla, D., Ravichandran, V., Schneider, B., Thanki, N., Weissig, H., Westbrook, J. D., and Zardecki, C. (2002) The Protein Data Bank, *Acta Crystallogr., Sect. D: Biol. Crystallogr. 58*, 899−907.

56. Fiser, A., Do, R. K., and Sali, A. (2000) Modeling of loops in protein structures, *Protein Sci. 9*, 1753−1773.

57. Shiu, S. H., and Bleecker, A. B. (2001) Receptor-like kinases from Arabidopsis form a monophyletic gene family related to animal receptor kinases, *Proc. Natl. Acad. Sci. U.S.A. 98*, 10763−10768.

58. Lichtarge, O., Bourne, H. R., and Cohen, F. E. (1996) An evolutionary trace method defines binding surfaces common to protein families, *J. Mol. Biol. 257*, 342−358.

59. Lichtarge, O., and Sowa, M. E. (2002) Evolutionary predictions of binding surfaces and interactions, *Curr. Opin. Struct. Biol. 12*, 21−27.

60. Hanks, S. K., and Hunter, T. (1995) Protein kinases 6. The eukaryotic protein kinase superfamily: kinase (catalytic) domain structure and classification, *FASEB J. 9*, 576−596.

61. Nuhse, T. S., Stensballe, A., Jensen, O. N., and Peck, S. C. (2004) Phosphoproteomics of the Arabidopsis plasma membrane and a new phosphorylation site database, *Plant Cell 16*, 2394−2405.

62. Oh, M. H., Ray, W. K., Huber, S. C., Asara, J. M., Gage, D. A., and Clouse, S. D. (2000) Recombinant brassinosteroid insensitive 1 receptor-like kinase autophosphorylates on serine and threonine residues and phosphorylates a conserved peptide motif in vitro, *Plant Physiol. 124*, 751−766.

63. Baldwin, R. L. (1986) Temperature dependence of the hydrophobic interaction in protein folding, *Proc. Natl. Acad. Sci. U.S.A. 83*, 8069−8072.

64. Baker, B. M., and Murphy, K. P. (1998) Prediction of binding energetics from structure using empirical parameterization, *Methods Enzymol. 295*, 294−315.

65. Noguchi, T., Fujioka, S., Choe, S., Takatsuto, S., Yoshida, S., Yuan, H., Feldmann, K. A., and Tax, F. E. (1999) Brassinosteroid-insensitive dwarf mutants of Arabidopsis accumulate brassino-steroids, *Plant Physiol. 121*, 743−752.

66. Vert, G., Nemhauser, J. L., Geldner, N., Hong, F., and Chory, J. (2005) Molecular mechanisms of steroid hormone signaling in plants, *Annu. Rev. Cell Dev. Biol. 21*, 177−201.

67. Wang, X., and Chory, J. (2006) Brassinosteroids regulate dissociation of BKI1, a negative regulator of BRI1 signaling, from the plasma membrane, *Science*.

68. Taylor, S. S., Haste, N. M., and Ghosh, G. (2005) PKR and eIF2alpha: integration of kinase dimerization, activation, and substrate docking, *Cell 122*, 823−825.

69. Huse, M., Muir, T. W., Xu, L., Chen, Y. G., Kuriyan, J., and Massague, J. (2001) The TGF beta receptor activation process: an inhibitor- to substrate-binding switch. *Mol. Cell 8*, 671−682.

70. Kay, L. E., Muhandiram, D. R., Wolf, G., Shoelson, S. E., and Forman-Kay, J. D. (1998) Correlation between binding and dynamics at SH2 domain interfaces, *Nat. Struct. Biol. 5*, 156−163.

71. Olejniczak, E. T., Zhou, M. M., and Fesik, S. W. (1997) Changes in the NMR-derived motional parameters of the insulin receptor substrate 1 phosphotyrosine binding domain upon binding to an interleukin 4 receptor phosphopeptide, *Biochemistry 36*, 4118−4124.

72. Lichtarge, O., Sowa, M. E., and Philippi, A. (2002) Evolutionary traces of functional surfaces along G protein signaling pathway, *Methods Enzymol. 344*, 536−556.

73. Morgan, D. H., Kristensen, D. M., Mittelman, D., and Lichtarge, O. (2006) ET Viewer: an application for predicting and visualizing functional sites in protein structures, *Bioinformatics*.

74. Mihalek, I., Res, I., and Lichtarge, O. (2006) Evolutionary trace report_maker: a new type of service for comparative analysis of proteins, *Bioinformatics 22*, 1656−1657.